

Journal of Materials Chemistry A

Accepted Manuscript



This article can be cited before page numbers have been issued, to do this please use: X. Zhang, L. Chen, J. Yun, X. Wang and J. Kong, *J. Mater. Chem. A*, 2017, DOI: 10.1039/C7TA01156C.



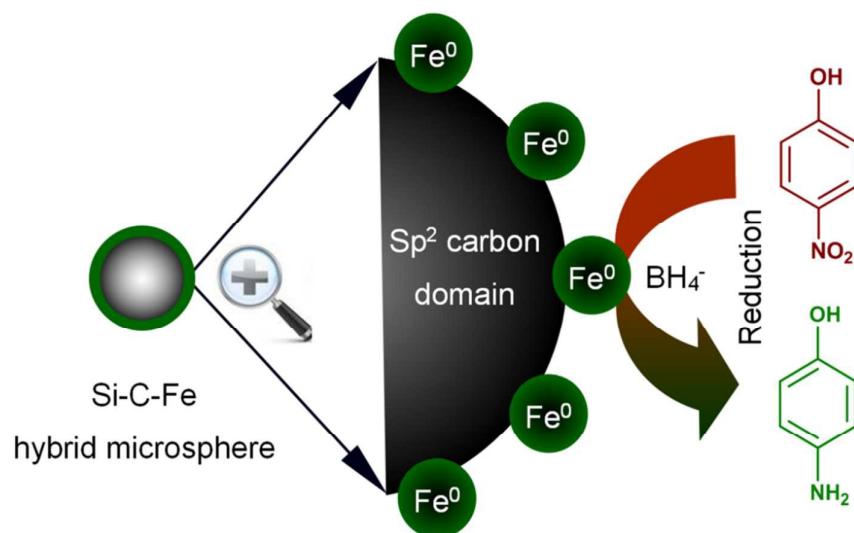
This is an Accepted Manuscript, which has been through the Royal Society of Chemistry peer review process and has been accepted for publication.

Accepted Manuscripts are published online shortly after acceptance, before technical editing, formatting and proof reading. Using this free service, authors can make their results available to the community, in citable form, before we publish the edited article. We will replace this Accepted Manuscript with the edited and formatted Advance Article as soon as it is available.

You can find more information about Accepted Manuscripts in the [author guidelines](#).

Please note that technical editing may introduce minor changes to the text and/or graphics, which may alter content. The journal's standard [Terms & Conditions](#) and the ethical guidelines, outlined in our [author and reviewer resource centre](#), still apply. In no event shall the Royal Society of Chemistry be held responsible for any errors or omissions in this Accepted Manuscript or any consequences arising from the use of any information it contains.

Table of Contents Entry



Constructing Magnetic Si-C-Fe Hybrid Microspheres for Room Temperature Nitroarenes Reduction

View Article Online
DOI: 10.1039/C7TA01156C

Xiaofei Zhang,^a Lixin Chen,^a Jin Yun,^a Xiaodong Wang,^{b,*} and Jie Kong^{a,*}

^aMOE Key Laboratory of Space Applied Physics and Chemistry, Shaanxi Key
Laboratory of Macromolecular Science and Technology, School of Science,
Northwestern Polytechnical University, Xi'an, 710072, P. R. China

^bSchool of Engineering, University of Aberdeen, Aberdeen AB24 3UE, Scotland, UK

Corresponding author e-mail addresses:

kongjie@nwpu.edu.cn (J.K.) and x.wang@abdn.ac.uk (X.W.)

Abstract:

In this work, we present the first synthesis and characterization of magnetic Si-C-Fe hybrid microspheres and their catalysis in room temperature reduction of 4-nitrophenol as a representative sustainable process of converting environmental pollutants to fine chemicals. The ferrocene-modified polydivinylbenzene (Fc-PDVB) precursor was synthesized by Pt-catalyzed hydrosilylation between the residual vinyl groups on PDVB surface and 1, 1'-bis(dimethylsilyl)ferrocene, where further pyrolysis led to the formation of Fe nanocrystals-containing Si-C-Fe hybrid microspheres. The precursor and hybrid microspheres were characterized in terms of transmission electron microscopy (TEM), Fourier transform infrared spectroscopy (FT-IR), BET surface area/porosity, powder X-ray diffraction (XRD), X-ray photoelectron spectroscopy (XPS), magnetic properties and MAS solid-state NMR measurements. The ultimate microspherical catalyst exhibited nano- and meso-pores, high specific surface area (i.e., $347.9 \text{ m}^2 \text{ g}^{-1}$) and good ferromagnetic properties. Efficient catalytic activity ($TOF: 0.163 \text{ s}^{-1}$), 100% selectivity (to 4-aminophenol) and excellent reusability (with easy separation) have been delivered. The achieved performance outperforms a number of nanomaterials such as supported noble metal particles, composites, monoliths and sheets. We have confirmed by DFT calculations that the activation of 4-nitrophenol via its weak non-covalent interaction with the sp^2 carbon domain of Si-C-Fe hybrid microspheres contributed to the superior performance which can be extended to a range of nitrobenzenes.

1. Introduction

Transition metal-containing polymers have received considerable attention in the past two decades due to their great potential in lithography, redox-active gels, molecular and ion recognition, liquid crystalline and supramolecular materials.¹⁻⁵ Hybrid materials or ceramics with porous structures can be generated by the emission of volatile species from cross-linked transition metal-containing polymers through moderate temperature pyrolysis (400–600 °C). It is evident that these hybrid materials or ceramics with incorporated transition metals exhibit not only improved optical, electrical, thermal and magnetic properties but also catalytic functionalities.⁶⁻⁹

Due to the above, transition metal-containing polymers are important precursors for the synthesis of metal-containing nanoparticles (NPs) if the polymerization and pyrolysis conditions are controlled.¹⁰⁻¹² In addition to the common cobalt (Co) and nickel (Ni)-containing NPs, various iron (Fe)-containing NPs¹³⁻¹⁵ have also been proven to possess excellent magnetic, electrical and catalytic properties, where ferrocene¹⁶ has been widely used as a precursor to synthesize carbon nanomaterials with Fe NPs. So far studies have been mainly focused on the pyrolysis of ferrocene-containing polymers like linear polyferrocenylsilanes (PFS), cross-linked PFS, PFS block copolymers, cobalt-clustered PFS, and hyperbranched PFS to obtain bulk materials,¹⁷⁻²¹ with little information on using ferrocene-containing polymers for the synthesis of materials at micro/nano-scale and particularly spherical materials. Owing to the spherical morphology, spherical materials have shown numerous real

and emerging applications.^{22,23} For example, spherical catalysts can be easily dispersed in the reaction solution and separated. In addition, spherical materials exhibit good mobility and high packing density that promote their use as the electrode materials.²⁴⁻²⁶

In this work, we propose for the first time the functionalization of readily available polydivinylbenzene (PDVB) particles (from precipitation polymerization, with significant surface residual vinyl groups²⁷⁻²⁹) by incorporating ferrocene to prepare ferrocene-containing polymer microspheres whose further pyrolysis can generate magnetic Si-C-Fe hybrid microspheres. This low-cost and recyclable magnetic material has been employed for the sustainable conversation of environmental pollutant 4-nitrophenol (4-NP) at room temperature. This is a critical reaction often chosen to evaluate the catalytic performance of metal nanoparticles,³⁰⁻³² since 4-NP has been a priority pollutant named by the U. S. Environmental Protection Agency due to its carcinogenic, anthropogenic and toxic nature and the target product 4-aminophenol (4-AP) is a chemical intermediate that is widely used in the synthesis of analgesic drugs such as acetaminophen, photographic developers, corrosion inhibitors and dyes.^{33,34} Most research on catalytic reduction of 4-NP has focused on noble metallic nanoparticles such as Au, Pd, Pt and Ag.³⁵⁻⁴³ The development of cheaper and efficient alternatives is always challenging.

2. Experimental

2.1 Materials

Divinylbenzene (m-and p-mixture, stabilized with 4-tert-butylcatechol), 2-amino-4-chloro-6-nitrophenol, 5-fluoro-2-nitrophenol, 1-bromo-4-nitrobenzene, 2-methoxy-5-nitrophenol, 2-methyl-5-nitrophenol, 1,2-dimethyl-4-nitrobenzene, n-butyllithium (1.6 M in hexane), N, N, N', N'-tetramethylethylenediamine (TMEDA), chlorodimethylsilane (98%), ferrocene (FeCp₂, 99%) and platinum-1,3-divinyl-1,1,3,3-tetramethyldisiloxane complex (Karstedt's catalyst, 0.1 M in polydimethylsiloxane terminated with vinyl groups), Fe powder, sodium borohydride (NaBH₄, > 97%) and 4-NP (> 99%) were supplied by J.&K. Sci. Co., Ltd. China. Toluene was distilled freshly under reflux by sodium/benzophenone. PDVB microspheres were synthesized according to previous report.⁴⁴ Chlorodimethylsilane and ferrocene were used to synthesis 1, 1'-bis(dimethylsilyl)ferrocene as described previously.⁴⁵

2.2 Synthesis and pyrolysis of ferrocene-modified PDVB microspheres

Under an argon (purity $\geq 99.999\%$) atmosphere, a dry flask was charged with PDVB microspheres (1 g), 1, 1'-bis(dimethylsilyl)ferrocene (4 g), 0.01g of Karstedt's catalyst and 150 mL of anhydrous toluene. After sufficient ultrasonic dispersing, the reaction mixture was stirred for 12 h at 80 °C under argon, the crude product was separated by vacuum filtration and washed three times successively with tetrahydrofuran, acetone and diethyl ether. A yellow sample was obtained after drying at 50 °C for 24 h in vacuum. Then, the as-prepared Fc-PDVB powder was loaded to a vertical tube furnace for (6 h) pyrolysis in argon (70 mL min⁻¹) at 500 °C, and cooled down to ambient temperature (at 5 °C min⁻¹). Finally, the Si-C-Fe hybrid microspheres

were obtained.

2.3 Characterization

Transmission electron microscopy (TEM, FEI, Tecnai G2 F20) was operated at 200 kV, coupled with electron diffraction analysis. Samples for analysis were dispersed in alcohol and deposited on a holey carbon/Cu grid (200 Mesh). Raman spectra were recorded using Raman Microprobe (Renishaw, UK) with 514.5 nm Ar⁺ laser excitation. UV-vis spectra were recorded using a spectrophotometer UV-2550 model (Shimadzu, Japan). Fourier Transform Infrared Spectroscopy (FT-IR) was measured using a Nicolet iSTO spectrometer (Varian, Palo Alto, California, USA) between 4000 to 400 cm⁻¹. The XPS spectra were recorded with a Kratos Axis 165 X-ray photoelectron spectrometer using a monochromatic Al K α radiation ($h\nu = 1486.6$ eV), at a take-off angle of 0°. All binding energy values were corrected to C 1s signal (285.0 eV). The pyrolysis of precursor was studied by thermogravimetric analysis (TGA) using STA 449 F3 thermoanalyzer with a ramp of 10 K min⁻¹ in argon (50 mL min⁻¹) between 40–1100 °C.

The MAS solid-state NMR measurements were carried out on a NMR spectrometer (Bruker Anance III-400, Germany). All spectra were acquired using magic angle spinning (MAS 54.74) technique with a rotation frequency of 6 kHz for ¹³C. All samples were measured with a crosspolarization sequence (CP). The recycle delay used was 3 s for ¹³C and the acquisition time was 42.3 ms for ¹³C. The ²⁹Si NMR

CP/MAS spectra were measured at a spinning speed of around 4.0 kHz, a contact time of 5 ms, and a recycle delay of 5 s.

View Article Online
DOI: 10.1039/C7TA01156C

X-ray diffractograms (XRD) were recorded on X9Pert Pro Powder diffractometer using Cu K α radiation (40 kV, 40 mA, PANalytical B.V., Netherlands). The specific surface area of selected samples was determined by N₂ adsorption–desorption isotherms at 195.8 °C using the commercial Micromeritics TriStar II 3020 and the Brunauer–Emmett–Teller (BET) method. Samples were outgassed at 150 °C for 24 h prior to measurements. The pore-size distribution was obtained using the adsorption isotherm and Barret-Joyner-Halender (BJH) method.

Magnetic properties of the samples were investigated by a commercial magnetic property measurement system (Quantum Design Inc., San Diego, USA). The magnetic behavior as a function of constant applied field (from -10 kOe to 10 kOe) was recorded at 300 K. ICP-MS (inductively coupled plasma mass spectrometry) was conducted on an Agilent 7700ce (Agilent Technologies, Santa Clara, CA, USA) using the aqueous solution.

2.4 Catalytic reduction of 4-nitrophenol (4-NP)

In a typical experiment, 2 mL of 4-NP aqueous solution (3 mM) was mixed with 10 mL fresh NaBH₄ solution (0.06 M). N₂ gas was then purged through the solution for 30 min to remove dissolved O₂. Subsequently, the N₂ flow was stopped and 4 mg as-prepared Si-C-Fe hybrid microspheres (or other catalysts) were added into the above solution (time $t = 0$ for reaction) under continuous agitation (at 200 rpm) at 298

K. Aliquots were removed from the reactor every minute and filtered through a 0.22 μm membrane filter for the determination of activity with UV-vis absorption spectroscopy. The composition of the product mixture was also analyzed by HPLC (LC-8A) equipped with a Welchrom[®] (C18, 5 μm , 4.6 \times 250 mm) column and SPD-20A UV-vis detector. Methanol, water and phosphate buffer (pH = 7) were employed as the mobile phase at a flow rate of 0.5 mL min⁻¹. After each reaction, the catalyst was separated and washed using 5 mL of 0.01 M NaBH₄ solution before the next experiment.

2.5 Computational details

Although there are considerable enhancements obtained over LDA and such conventional hybrid density functional theory (DFT) as B3LYP recently,^{46,47} it is still challenging to describe accurately non-covalent weak interaction systems in DFT. The hybrid functional M06-2X, developed by Truhlar *et al.*⁴⁸ provides relatively reliable results for π - π stacking systems.⁴⁹ Therefore, in this paper, all geometric optimizations were performed at M06-2X/6-311+g(d,p) level with the D3 version of Grimme's dispersion correction by using the Gaussian 09 program.

3. Results and Discussion

3.1 Synthesis and characterization of ferrocene-modified PDVB microspheres

The synthesis route of Fc-PDVB microspheres is illustrated in **Scheme 1**. They were obtained via the hydrosilylation between vinyl groups on the surface of PDVB microspheres and 1,1'-bis(dimethylsilyl)ferrocene. As previously reported,⁵⁰ the

olefin was considered as a nucleophile and thus the Pt colloid/ R_3SiH intermediate from the reaction of the Pt colloid and R_3SiH was an electrophile in this reaction. So the ferrocenyl substituent which has electron donating characteristics in 1,1'-bis(dimethylsilyl)ferrocene has an adverse impact on hydrosilylation, while the electron donating ability of phenyl makes vinyl groups on the surface of PDVB microspheres display a faster rate of hydrosilylation. Normally, the reaction hardly occurred when temperature was lower than 50 °C. With increasing temperature from 50 to 80 °C, the reaction was initiated and consequently the color of as-prepared Fc-PDVB microspheres changed from light yellow to orange. According to PDVB microspheres formation mechanism,⁵¹ PDVB microspheres have a thin surface layer consisting of lightly crosslinked and swellable poly(divinylbenzene), and at high temperature (80 °C), toluene can lead to swollen surface layer of PDVB microspheres so that the 1,1'-bis(dimethylsilyl)ferrocene can penetrate into every space among the polymer chains, giving it more chance to react with double bond from the surface of PDVB microspheres, even in the interior. The TEM images in **Fig. 1** show well-defined, smooth and uniform Fc-PDVB microspheres with an average diameter of about 2 μm and morphology which is similar to that of the original PDVB microspheres. This confirms the preparation procedure (e.g., washing) is sufficient in removing any unreacted 1,1'-bis(dimethylsilyl)ferrocene and Karstedt's catalyst on the surface of microspheres by physical adsorption.

In **Fig. 2**, the FT-IR characteristic peak at 1254 cm^{-1} corresponds to the asymmetric deformation vibration of the Si-CH₃ and the out-of-plane CH bending vibration of Cp

is observed at 1165 and 1035 cm^{-1} . In addition, the peak of Si-H at 2113 cm^{-1} decreases significantly, which indicates that Si-H groups from 1, 1'-bis-(dimethylsilyl)ferrocene reacted with vinyl groups. Due to the influence of aromatic structures from PDVB segments and ferrocenyl units, it is difficult to determine the decrease of the absorption peak intensity of double bonds located on the surface of PDVB microspheres from FT-IR spectra. We therefore employed the MAS solid-state NMR to probe this and the ^{13}C CP/MAS NMR and ^{29}Si NMR spectra are shown in **Fig. 3** along with the peak assignments according to the literature.^{52,53} In comparison to the original PDVB microspheres, the ferrocene-modified ones show decreased intensity of the signals at 137.3 and 112.4 ppm for the carbon atoms of $\text{CH}=\text{CH}_2$, demonstrating the consumption of double bonds located on the surface of PDVB. The increased intensity of the peak at 29.5 ppm from CH_2Ph shows the generation of $\text{SiCH}_2\text{CH}_2\text{Ph}$ from β -addition hydrosilylation. The intensity of the peak at 15.5 ppm from $\text{C}-\text{CH}_3$ is not increased, which means that no α -adducts were obtained. In another words, the hydrosilylation between carbon-carbon double bonds on the PDVB surface and 1, 1'-bis-(dimethylsilyl)ferrocene is conducted in β -addition regime. In addition, the chemical shifts at 71.9, 68.9 and -2.4 ppm clearly show the existence of Cp and $\text{Si}-\text{CH}_3$, which further confirms the occurrence of hydrosilylation. Similarly, in the ^{29}Si NMR spectrum (**Fig. 3**), it is evident that there are two types of silicon atoms. The first one, $\delta = -0.1$ ppm, is correlated with $\text{Si}-\text{CH}_2$ from the 1, 1'-bis-(dimethylsilyl)ferrocene on the PDVB surface after hydrosilylation. The second one, $\delta = -19.8$ ppm, can be assigned to the chemical shift of unreacted Si-H

groups on the other side of 1, 1'-bis-(dimethylsilyl)ferrocene. These results further confirm that our hydrosilylation between vinyl groups on the surface of PDVB microspheres and 1,1'-bis(dimethylsilyl)ferrocene has a high regioselectivity, whereas it was reported in the literature that both α - and β -isomers might be obtained in other hydrosilylation systems.⁵⁴ This can be attributed to the remarkable steric hindrance of phenyl and ferrocenyl, which have unfavorable influences on attack between Pt colloid/R₃SiH intermediate and methine carbon on double bonds. In addition, owing to the weak electron-withdrawing inductive effect of phenyl on double bonds, the electron density of methylene carbon is higher than that of methine carbon, which makes the latter easier for attack by an electrophile to form β -addition.

The surface characteristics of Fc-PDVB microspheres were evaluated by XPS analysis (**Fig. 4**) and the associated atomic composition can be found in **Table 1**. All the silicon, carbon, oxygen and iron elements are evident on the surface. The Si 2p peak can be deconvoluted into the C-Si and C-Si-O peaks and the C1s peak can be deconvoluted into the C=C and C-C, C-O-H, and C=O peaks. The Fe 2p spectrum shows two peaks that can be assigned to Fe 2p_{3/2} and Fe 2p_{1/2} in the ferrocene unit, respectively. These are consistent with comparable systems reported in the literature.⁵⁵⁻⁵⁷ The presence of oxygen on the surface of microspheres is mainly due to the moisture and O₂ absorbed by the samples before measurement. In summary, the FT-IR, ¹³C and ²⁹Si CP/MAS NMR and XPS results have provided fundamental details on the structure of ferrocene-modified PDVB microspheres after surface hydrosilylation.

3.2 Pyrolysis of ferrocene-modified PDVB microspheres and characterization of the produced materials

As can be seen from the TGA curves in **Fig. 5**, the 1,1'-bis-(dimethylsilyl)ferrocene is almost totally sublimated or evaporated after around 200 °C. For the original PDVB microspheres, a rapid thermolytic degradation in the temperature range of 400-600 °C can be observed, after which the TGA curve almost levels off. In comparison to this, the yield upon heat treatment of the Fc-PDVB microspheres is slightly increased. This is due to the better thermal stability of ferrocenylsilane units introduced by the hydrosilylation of 1,1'-bis-(dimethylsilyl)ferrocene. **Fig. 6** shows the simultaneous TGA and mass spectrometry results of the Fc-PDVB microspheres. Similar to the original PDVB microspheres, the thermolysis of Fc-PDVB microspheres is mainly accompanied by the evolutions of H₂ (m/z=2), hydrocarbons CH_x (x=1-3, m/z=13-15), CH₄ (m/z=16), H₂O (m/z=18), CHCH (m/z=26), CH₂CH₂ (m/z=28), CHCHC (m/z=38), CH₃CHO (m/z=44) and oligomer fragments (m/z=50, 52, 63 and 74).

The evolution of CH₄ and/or hydrocarbons between 300 and 600 °C can be attributed to the decomposition of Si-CH₃ groups and cleavage of C-C bonds. An ionized group with mass of 12 is observed, resulting from carbon monoxide and carbon dioxide.

Oxygen, which allows the oxidation of samples to produce CO, H₂O, and CO₂ at high temperature, originates from the moisture content absorbed by the microspheres' surface. However, the thermolysis behavior of Fc-PDVB microspheres is noticeably different from that of PDVB microspheres, with the decomposition of Si-CH₃ and Cp,

the CH₃ (m/z=15), CHCHC (m/z=38) and oligomer fragment (m/z=52) evolutions

View Article Online
DOI: 10.1039/C7TA01156C

becomes stronger than that of PDVB microspheres at 350-700 °C. In contrast, the evolution of C (m/z=12), OH (m/z=17), H₂O (m/z=18) and CO₂ (m/z=44) from the pyrolysis of Fc-PDVB microspheres is decreased significantly. This can be attributed to the fact that the formation of Fc-PDVB microspheres has consumed the vinyl groups (easy to oxidize) on the PDVB surface.

The pyrolyzed microspheres from Fc-PDVB at 500 °C in argon were further characterized by XPS as shown in **Fig. 7**. The summary of binding energy of different chemical bonds is given in **Table 2**, where detailed assignment of spectra can be found in the literature.⁵⁸⁻⁶¹ Besides C-Si, C=C, C-C, some oxygen-related bonds, such as Si-O, C-O, C-OH, C=O and COOH can also be found. For the Fe 2p spectrum, the peaks at 707.5 eV, 709.6 eV and 712.0 eV represent the binding energies of Fe⁰ 2p_{3/2}, Fe²⁺ 2p_{3/2} and FeOOH 2p_{3/2}, respectively. These different oxidation states could be produced by the surface oxidation of Fe⁰ by the moisture adsorbed. XPS analysis indicates that the pyrolyzed microspheres exhibit a Si-C-Fe hybrid structure which is also confirmed by the XRD results (see **Fig. S1(a)†**) indicating the formation of Fe nanocrystals (ICSD, PDF#06-0696) in the microspheres. As shown in the XPS results, the major ingredient of Si-C-Fe hybrid microspheres is free carbon, and therefore Raman spectroscopy as an efficient tool for the examination of the structure of free carbons was used to study the structural information of the free carbon in Si-C-Fe hybrid microspheres. The Raman spectra (see **Fig. S1(b)†**) exhibit a broad absorption peak at 1355 cm⁻¹ and a sharp one at 1580 cm⁻¹, corresponding to carbon vibration of

the D and G bands, respectively. The former one is ascribed to sp^3 carbons while the latter originates from in-plane bond stretching of sp^2 carbon.⁶² The strong absorption peak at 1580 cm^{-1} suggests the present of large number of sp^2 -bonded carbons in Si-C-Fe hybrid microspheres.

Representative TEM images of Si-C-Fe hybrid microspheres are shown in **Fig. 8**. Compared with Fc-PDVB microspheres (**Fig. 1b**), the size of the pyrolyzed samples became smaller because of sharp shrinkage during the transformation of the organic network of Fc-PDVB microspheres to organic-inorganic Si-C-Fe hybrid microspheres. In addition, nanoscale Fe-rich region (diameter of $\sim 10\text{ nm}$) is evident in the higher magnification TEM image. The measured d (110) spacing of Fe is 0.203 nm that is consistent with the value obtained from XRD measurement and the literature. This further confirms the presence of Fe^0 . The nitrogen physisorption measurements of the pyrolyzed microspheres in **Fig. 9** exhibit a type I isotherm, which is typical for nano- and meso-porous structures with a specific surface area of $347.9\text{ m}^2\text{ g}^{-1}$. A large nitrogen uptake at low relative pressure ($p/p^0 < 0.05$) indicates the presence of significant fraction of micropores below 20 \AA . The formation of porous structures can be resulted from the evolutions of gases (see **Fig. 6**) during the transformation of organic to inorganic microspheres.

The magnetic properties of the Si-C-Fe hybrid microspheres have been studied and the magnetization curve is presented in **Fig. 10**. In the magnetic field at 300 K , the pyrolyzed microspheres are swiftly magnetized with an immediate rise in its

magnetization curve and the saturation magnetization was 2.4 emu g^{-1} . In the enlarged magnetization curve in the low-field region, the Si-C-Fe hybrid microspheres exhibit hysteresis loops with low small remanent magnetization (0.31 emu g^{-1}). This indicates Si-C-Fe hybrid microspheres have soft ferromagnetism at room-temperature which is similar to the Si/C/Fe ceramic material containing Fe^0 nanoparticles.⁶³ This result further confirms the formation of Fe^0 nanocrystals in Si-C-Fe hybrid microspheres which is in line with previous analyses. To summarize, Si-C-Fe hybrid microspheres containing nanocrystalline Fe^0 and significant regions of sp^2 -bonded carbons were prepared successfully by Fc-PDVB microspheres pyrolysis with high specific surface area and good ferromagnetism.

3.3 Catalytic response

The reduction of 4-NP by NaBH_4 was chosen as a model reaction to evaluate the catalytic performance of Si-C-Fe hybrid microspheres in pollutant treatment for environmental sustainability. A series of control experiments have been conducted to benchmark the results in this work. We first excluded the possibility of any reaction taking place in the absence of catalyst as shown in **Fig. S2†**. It is well established that 4-NP solution exhibits a strong absorption peak at 400 nm after addition of an aqueous solution of NaBH_4 .^{64,65} The intensity of the absorption peak at 400 nm showed no significant decrease (in 5 min) and the characteristic peak of 4-AP did not appear even at prolonged period (i.e., 100 min, see **Fig. S2†**). This means that there is no reduction happening as a result of the repulsion between the negatively charged

BH_4^- and ionized 4-NP (i.e., 4-nitrophenolate ions).⁶⁶ Su and coworkers have reported previously that pure carbon materials also exhibit catalytic activity in nitrobenzene reduction (by hydrazine hydrate)⁷¹⁻⁷³ We then considered whether the carbon components in our catalyst are active as there is a large amount of carbon in the Si-C-Fe hybrid microspheres according to the XPS and Raman results (see **Fig. 7** and **Fig. S1b†**). To check this, carbon microspheres were prepared by the pyrolysis of pure PDVB microspheres (i.e., with no Fe or Si) under the same conditions and examined. The results show that the pyrolyzed PDVB microspheres exhibit no catalytic activity in 4-NP reduction (**Fig. S3†**), attributable to the absence of active sites like C-O, -COO-, C-O-B, B=O, B-O, C-B groups on the surface of our catalysts (prepared/treated in an inert Ar atmosphere). The same response was also observed over the Si-C hybrid materials (pyrolyzed product of silicon and acetylene polymer heated at 773 K, i.e., with no Fe)

Fig. 11(a) shows the successive UV-Vis spectra of aqueous solutions containing 4-NP and NaBH_4 in the presence of Si-C-Fe hybrid microspheres. By adding a small amount (4 mg) of magnetic Si-C-Fe microspheres as catalyst, the absorption peak at 400 nm disappeared completely (i.e., 100% conversion, **Fig. 11(b)**) in 5 min with a simultaneous increase in the characteristic peak of 4-AP. The appearance of a colorless solution (from yellow), indicated that only the conversion of 4-NP into 4-AP was achieved (i.e., 100% selectivity).^{40,67} Since NaBH_4 was used in excess, the reduction of 4-NP can be considered as a first order reaction and the following kinetics is applicable.

$$\ln(C_t/C_0) = -k_{app}t \text{ (or } \ln(A_t/A_0) = -k_{app}t)$$

where C_t is the concentration of 4-NP at time t and k_{app} is the apparent rate constant.

k_{app} can then be normalized to the concentration of Fe deriving k_{nor} .^{68,69} **Fig. 11(c)**

shows $\ln(A_t/A_0)$ as a function reaction time over Si-C-Fe hybrid microspheres, where

k_{app} and k_{nor} obtained are $19.27 \times 10^{-3} \text{ s}^{-1}$ and $0.326 \text{ s}^{-1} \text{ mM}^{-1}$ (using a Fe content of

0.99 wt% (from ICP analysis)), respectively. In order to investigate the intrinsic

catalytic response, it is necessary to establish reaction conditions under

kinetic/chemical control wherein transport constraints are minimized. A nearly

proportional change (8.05 , 19.27 and $36.73 \times 10^{-3} \text{ s}^{-1}$) in the apparent rate constant

(**Fig. 11(c) and S4†**) with changing catalyst mass (2, 4 and 8 mg) has been observed,

demonstrating negligible interphase diffusional limitations. Subsequent tests were

thus conducted using 4 mg of catalyst. To further demonstrate the potential of the

synthesized Si-C-Fe microspheres in catalysis, a harsher reaction condition, i.e.,

sub-ambient temperature, 273 K, was considered and it is stimulating to notice that

the catalyst can still promote the target reaction, although at a lower rate ($k_{app} = 4.49 \times$

10^{-3} s^{-1} , see **Fig. S5†**).

Initial turnover frequency (*TOF*, moles of 4-NP converted per mole of Fe per second)

can be calculated using the obtained k_{app} . The performance (under comparable

conditions) of different metal nanocatalysts employed for the reduction of 4-NP have

been summarized in **Table 3**. It is noteworthy that our system has outperformed most

of the recent catalysts reported including noble metals (Pd, Pt, Au and Ag)^{31,39-43} in

various forms (e.g., nanoparticles, nanocomposites, etc.) and is ~20% more active

(0.163 s^{-1} vs. 0.136 s^{-1}) than the work employing nanosheet array-like Cu catalyst ($\text{Cu}_x\text{Mg}_{3-x}\text{Al}$ -layered double hydroxide/reduced graphene oxide) reported very recently.⁷⁰ Moreover, the magnetic Si-C-Fe microspheres can be easily separated from the reaction system by an external magnet for reuse (see **Fig. 11(b)**) and the recycled catalyst exhibited similar high activity in five successive cycles (see **Fig. 11(d)**), demonstrating excellent reusability. These results suggest an interesting development in novel catalyst formulations for room and sub-ambient temperature pollution abatement.

In addition to the high surface area and well dispersed Fe^0 (as active sites⁷⁴ and **Fig. S6†**) on the surface of Si-C-Fe hybrid microspheres (see characterization) that are beneficial for catalysis, we also consider that the non-covalent interaction between 4-NP and the sp^2 carbon domain (see Raman spectra in **Fig. S1b†**) is the main reason for the high activity achieved. It is such interaction that gathers 4-NP on the surface of Si-C-Fe hybrid microspheres, accessible to the active sites. This consideration is based on previous reports that the intimate interaction between graphene (sp^2 carbon) and aromatic derivatives due to their π -character may make the reactants easily accessible to the active sites of noble metal.^{75,76} In order to confirm the presence of such interaction in our system, quantum chemical DFT calculations were carried out. The optimized structures of 4-NP, sp^2 carbon domain and their mixture are shown in **Fig. 12**. The calculated atomic distance between the carbons of 4-NP and sp^2 carbon domain of Si-C-Fe hybrid microspheres is about 3.1-3.4 Å which is within the typical range of van der Waals distance (3–4 Å).⁷⁷ This demonstrates that the

concentration/activation of 4-NP on the catalyst surface can be related to van der Waals forces between sp^2 carbons domain and 4-NP, i.e., weak non-covalent interaction.

To ensure the general applicability of our catalyst in converting environmental pollutants into useful chemicals, a series of nitroarenes with different substituent groups were also considered. The results (see **Table 4**) illustrate that the Si-C-Fe hybrid microspheres exhibit efficient catalytic activity to selectively reduce nitroarenes with different functionalities, showing great potential as an alternative to the noble metal catalytic materials.

4. Conclusions

In summary, ferrocene-modified PDVB microspheres were successfully synthesized by the hydrosilation between the residual vinyl groups on the PDVB surface and 1, 1'-bis (dimethylsilyl)ferrocene. The pyrolysis of ferrocene-modified PDVB microspheres resulted in the formation of novel Fe nanocrystal-containing Si-C magnetic microspheres which exhibited nano- and meso-porous structures, large surface area, good ferromagnetic properties and superior catalytic activity (due to the weak non-covalent interaction) in the reduction of a series of nitrobenzenes with a reusability feature. The results in this study provide a convenient strategy for the synthesis of low cost, magnetic, hybrid microspherical materials with catalysis functionalities, which may find wide applications in sustainable conversion of environmental pollutants as well as chemical intermediates production.

View Article Online
DOI: 10.1039/C7TA01156C

Acknowledgments

This research is supported by the National Natural Science Foundation of China (21174112). X.W. acknowledges support from School of Engineering, the University of Aberdeen. The useful discussion with Dr. M.D. Symes (University of Glasgow) is gratefully acknowledged.

Notes and References

- 1 G. R. Whittell, M. D. Hager, U. S. Schubert, I. Manners, *Nat. Mater.*, 2011, **10**, 176-188.
- 2 K. Liu, C. L. Ho, S. Aouba, Y. Q. Zhao, Z. H. Lu, P. Srebri, N. Coombs, P. Dube, H. E. Ruda, W. Y. Wong, I. Manners, *Angew. Chem. Int. Ed.*, 2008, **47**, 1255-1259.
- 3 M. A. Hempenius, C. Cirimi, F. L. Savio, J. Song, G. J. Vancso, *Macromol. Rapid Commun.*, 2010, **31**, 772-783.
- 4 R. Ahmed, A. Priimagi, C. F. J. Faul, I. Manners, *Adv. Mater.*, 2012, **24**, 926-931.
- 5 Q. Sun, J. W. Y. Lam, K. Xu, H. Xu, J. A. K. Cha, P. C. L. Wong, G. Wen, X. Zhang, X. Jing, F. Wang, B. Z. Tang, *Chem. Mater.*, 2000, **12**, 2617-2624.
- 6 Q. Li, X. Yin, W. Duan, L. Kong, X. Liu, L. Cheng, L. Zhang, *J. Eur. Ceram. Soc.*, **2014**, 34, 2187-2201.
- 7 M. Zaheer, T. Schmalz, G. Motz, R. Kempe, *Chem. Soc. Rev.*, 2012, **41**, 5102-5116.
- 8 M. Zaheer, C. D. Keenan, J. Hermannsdörfer, E. Roessler, G. Motz, J. Senker, R. Kempe, *Chem. Mater.*, 2012, **24**, 3952-3963.
- 9 M. Hojamberdiev, R. M. Prasad, K. Morita, M. A. Schiavonc, R. Riedel, *Micropor. Mesopor. Mater.*, 2012, **151**, 330-338.
- 10 L. Ren, J. Zhang, C. G. Hardy, S. Ma, C. Tang, *Macromol. Rapid Commun.*, 2012, **33**, 510-516.
- 11 R. Fu, T. F. Baumann, S. Cronin, G. Dresselhaus, M. S. Dresselhaus, J. H. Satcher Jr, *Langmuir*, 2005, **21**, 2647-2651.

- 12 W. Y. Chan, S. B. Clendenning, A. Berenbaum, A. J. Lough, S. Aouba, H. E. Ruda, *J. Am. Chem. Soc.*, 2005, **127**, 1765-1772.
- 13 H. M. T. Galvis, J. H. Bitter, C. B. Khare, M. Ruitenbeek, A. I. Dugulan, K. P. de Jong, *Science*, 2012, **335**, 835-838.
- 14 C. Lee, J. Y. Kim, W. I. Lee, K. L. Nelson, J. Yoon, D. L. Sedlak, *Environ. Sci. Technol.*, 2008, **42**, 4927-4933.
- 15 Y. Xu, D. Zhao, *Water Res.*, 2007, **41**, 2101-2108.
- 16 Y. Lu, Z. Zhu, Z. Liu, *Carbon*, 2005, **43**, 369-374.
- 17 K. Liu, S. B. Clendenning, L. Friebe, W. Y. Chan, X. Zhu, M. R. Freeman, G. C. Yang, C. M. Yip, D. Grozea, Z. H. Lu, I. Manners, *Chem. Mater.*, 2006, **18**, 2591-2601.
- 18 D. A. Rider, K. Liu, J. C. Eloi, L. Vanderark, L. Yang, J. Y. Wang, D. Grozea, Z. H. Lu, T. P. Russell, I. Manners, *ACS Nano*, 2008, **2**, 263-270.
- 19 N. McGrath, F. H. Schacher, H. Qiu, S. Mann, M. A. Winnik, I. Manners, *Polym. Chem.*, 2014, **5**, 1923-1929.
- 20 K. Temple, K. Kulbaba, K. N. Power-Billard, I. Manners, K. A. Leach, T. Xu, T. P. Russell, C. J. Hawker, *Adv. Mater.*, 2003, **15**, 297-300.
- 21 J. Shi, B. Tong, Z. Li, J. Shen, W. Zhao, H. Fu, J. Zhi, Y. Dong, M. Häussler, J. W. Y. Lam, B. Z. Tang, *Macromolecules*, 2007, **40**, 8195-8204.
- 22 M. Xie, X. Dai, S. Meng, X. Fu, S. Chen, *Chem. Eng. J.*, 2014, **245**, 107-116.
- 23 R. Nan, Y. H. Yang, S. Jiang, Y. H. Zhang, H. L. Xu, G. Zi, Y. Tang, *J. Catal.*, 2007, **251**, 182-188.
- 24 C. Zhang, Z. Chen, Z. Guo, X. W. D. Lou, *Energ. Environ. Sci.*, 2013, **6**, 974-978.
- 25 Z. Ju, C. Guo, Y. Qian, B. Tang, S. Xiong, *Nanoscale*, 2014, **6**, 3268-3273.
- 26 J. Zhou, J. Lian, L. Hou, J. Zhang, H. Gou, M. Xia, Y. Zhao, T. A. Strobel, L. Tao, F. Gao, *Nat. Commun.*, 2015, **6**, 8503.
- 27 I. Koprinarov, A. P. Hitchcock, W. H. Li, Y. M. Heng, H. D. H. Stöver, *Macromolecules*, 2001, **34**, 4424-4429.
- 28 J. S. Downey, R. S. Frank, W. H. Li, H. D. H. Stöver, *Macromolecules*, 1999, **32**, 4424-4429.

- 32**, 2838-2844.
- 29 W. H. Li, H. D. H. Stöver, *Macromolecules*, 2000, **33**, 4354-4360.
- 30 J. Zeng, Q. Zhang, J. Chen, Y. Xia, *Nano Lett.*, 2009, **10**, 30-35.
- 31 P. Zhang, C. Shao, Z. Zhang, M. Zhang, J. Mu, Z. Guo, Y. Liu, *Nanoscale*, 2011, **3**, 3357-3363.
- 32 S. Saha, A. Pal, S. Kundu, S. Basu, T. Pal, *Langmuir*, 2010, **26**, 2885-2893.
- 33 S. K. Tanielyan, J. J. Nair, N. Marin, G. Alvez, R. J. McNair, D. Wang, R. L. Augustine, *Org. Process Res. Dev.*, 2007, **11**, 681-688.
- 34 J. F. Corbett, *Dyes Pigments*, 1999, **41**, 127-136.
- 35 S. Gao, Z. Zhang, K. Liu, B. Dong, *Appl. Catal. B: Environ.*, 2016, **188**, 245-252.
- 36 X. Gu, W. Qi, X. Xu, Z. Sun, L. Zhang, W. Liu, X. Pan, D. S. Su, *Nanoscale*, 2014, **6**, 6609-6616.
- 37 P. Zhao, X. Feng, D. Huang, G. Yang, D. Astruc, *Coordin. Chem. Rev.*, 2015, **287**, 114-136.
- 38 M. A. Mahmoud, M. A. El-Sayed, *ChemCatChem*, 2014, **6**, 3540-3546.
- 39 M. Zhu, C. Wang, D. Meng, G. Diao, *J. Mater. Chem. A*, 2013, **1**, 2118-2125.
- 40 Y. Fang, E. Wang, *Nanoscale*, 2013, **5**, 1843-1848.
- 41 H. Liu, D. Wan, D. Jiang, J. Ming, *ACS Appl. Mater. Interfaces*, 2015, **7**, 20885-20892.
- 42 M. Tang, G. Huang, X. Li, X. Pang, H. Qiu, *Mater. Chem. Phys.*, 2015, **162**, 31-40.
- 43 W. Hu, B. Liu, Q. Wang, Y. Liu, Y. Liu, P. Jing, S. Yu, L. Liu, J. Zhang, *Chem. Commun.*, 2013, **49**, 7596-7598.
- 44 F. Bai, X. Yang, W. Huang, *Macromolecules*, 2004, **37**, 9746-9752.
- 45 R. Jain, H. Choi, R. A. Lalancette, J. B. Sheridan, *Organometallics*, 2005, **24**, 1468-1476
- 46 X. Xu, W.A. Goddard III, *Proc. Natl. Acad. Sci. U.S.A.*, 2004, **101**, 2673-2677.
- 47 H. Tachikawa, H. Kawabata, *J. Phys. Chem. C*, 2009, **113**, 7603-7609.

- 48 Y. Zhao, N.E. Schultz, G.D. Truhlar, *J. Chem. Theory Comput.*, 2006, **2**, 364–382.
- 49 W. Sun, Y. Bu, Y. Wang, *J. Phys. Chem. C*, 2011, **115**, 3220–3228.
- 50 L. N. Lewis. *J. Am. Chem. Soc.*, 1990, **112**, 5998-6004.
- 51 J. S. Downey, G. McIsaac, R. S. Frank, H. D. H. Stöver, *Macromolecules*, 2001, **34**, 4534-4541.
- 52 M. Gaborieau, L. Nebhani, R. Graf, L. Barner, C. Barner-Kowollik, *Macromolecules*, 2010, **43**, 3868-3875.
- 53 J. Kong, T. Schmalz, G. Motz, A. H. E. Müller, *Macromolecules*, 2011, **44**, 1280-1291.
- 54 S. J. Wang, X. D. Fan, J. Kong, J. R. Lu, *Polymer*, 2009, **50**, 3587-3594.
- 55 G. Zhang, S. Sun, D. Yang, J. P. Dodelet, E. Sacher, *Carbon*, 2008, **46**, 196-205.
- 56 L. L. Meng, X. F. Zhang, Y. S. Tang, K. H. Su, J. Kong, *Sci. Rep.*, 2015, **5**, 7910.
- 57 C. M. Woodbridge, D. L. Pugmire, R. C. Johnson, N. M. Boag, M. A. Langell, *J. Phys. Chem. B*, 2000, **104**, 3085-3093.
- 58 J. R. Waldrop, R. W. Grant, Y. C. Wang, R. F. Davis, *J. Appl. Phys.*, 1992, **72**, 4757-4760.
- 59 W. F. Zhao, Y. S. Tang, J. Xi, J. Kong, *Appl. Surf. Sci.*, 2015, **326**, 276-284.
- 60 V. Stambouli, C. Palacio, H. J. Mathieu, D. Landolt, *Appl. Surf. Sci.*, 1993, **70**, 240-244.
- 61 J. Kong, M. J. Wang, J. H. Zou, L. N. An, *ACS Appl. Mater. Interfaces*, 2015, **7**, 6733-6744.
- 62 S. Karlin, P. Colomban, *J. Raman Spectrosc.*, 1997, **28**, 219-228.
- 63 Z. Yu, L. Yang, H. Min, P. Zhang, C. Zhou, R. Riedel, *J. Mater. Chem. C*, 2014, **2**, 1057-1067.
- 64 J. Zeng, Q. Zhang, J. Chen, Y. Xia, *Nano Lett.*, 2010, **10**, 30-35.
- 65 K. Hayakawa, T. Yoshimura, K. Esumi. *Langmuir*, 2003, **19**, 5517-5521.
- 66 D. Xu, P. Diao, T. Jin, Q. Wu, X. Liu, X. Guo, H. Gong, F. Li, M. Xiang, R. Yu,

- ACS Appl. Mater. Interfaces*, 2015, **7**, 16738-16749.
- 67 P. Zhang, R. Li, Y. Huang, Q. Chen, *ACS Appl. Mater. Interfaces*, 2014, **6**, 2671-2678.
- 68 T. Yu, J. Zeng, B. Lim, Y. Xia, *Adv. Mater.*, 2010, **22**, 5188-5192.
- 69 M. Rashid, TK Mandal. *Adv. Funct. Mater.*, 2008, **18**, 2261-2271.
- 70 L. Dou, H. Zhang, *J. Mater. Chem. A*, 2016, **4**, 18990-19002.
- 71 S. Wu, G. Wen, R. Schlögl, D. S. Su, *Phys. Chem. Chem. Phys.*, 2015, **17**, 1567-1571.
- 72 Y. Lin, S. Wu, W. Shi, B. Zhang, J. Wang, Y. A. Kim, M. Endo, D. S. Su, *Chem. Commun.*, 2015, **51**, 13086-13089.
- 73 S. Wu, G. Wen, B. Zhong, B. Zhang, X. Gu, N. Wang, D. S. Su, *Chin. J. Catal.* 2014, **35**, 914-921.
- 74 S. Bae, K. Hanna, *Environ. Sci. Technol.*, 2015, **49**, 10536-10543.
- 75 R. Nie, J. Shi, W. Du, W. Ning, Z. Hou, F. S. Xiao, *J. Mater. Chem. A*, 2013, **1**, 9037-9045.
- 76 J. H. Yang, G. Sun, Y. Gao, H. Zhao, P. Tang, J. Tan, A. Lu, D. Ma, *Energ. Environ. Sci.*, 2013, **6**, 793-798.
- 77 P. Sutter, J. T. Sadowski, E. Sutter, *Phys. Rev. B*, 2009, **80**, 308-310.

Table, Scheme and Figure Captions:

Table 1 The binding energy (B.E.) of chemical bonds of ferrocene-modified PDVB microspheres.

Table 2 The binding energy (B.E.) of chemical bonds of the synthesized Si-C-Fe hybrid microspheres.

Table 3 Comparison of catalytic performance by various metal nanocatalysts for the reduction of 4-nitrophenol.

Table 4 Catalytic performance of Si-C-Fe hybrid microspheres in the reduction of various nitroarenes (to the corresponding amines).^a

Scheme 1 The synthesis scheme of ferrocene-modified PDVB microspheres by the hydrosilylation between vinyl groups on the surface of PDVB microspheres and 1, 1'-bis(dimethylsilyl)ferrocene.

Fig. 1 TEM images of PDVB microspheres (a) and ferrocene-modified PDVB microspheres (b).

Fig. 2 The FT-IR spectra of ferrocene-modified PDVB microspheres (a), PDVB microspheres (b) and 1, 1'-bis-(dimethylsilyl)ferrocene (c).

Fig. 3 ^{13}C CP/MAS NMR spectra of ferrocene-modified PDVB microspheres (red line) and PDVB microspheres (black line), and ^{29}Si CP/MAS NMR spectrum of ferrocene-modified PDVB microspheres (green line).

Fig. 4 XPS spectra of ferrocene-modified PDVB microspheres after surface hydrosilylation of microspheres and 1, 1'-bis(dimethylsilyl)ferrocene.

Fig. 5 The thermalgravimetry curves of ferrocene-modified PDVB microspheres (a), original PDVB microspheres (b) and 1, 1'-bis-(dimethylsilyl)ferrocene (c).

Fig. 6 The simultaneous TGA and mass spectrometry results of ferrocene-modified PDVB microspheres (a) and original PDVB microspheres (b).

Fig. 7 The XPS spectra of the synthesized Si-C-Fe hybrid microspheres.

Fig. 8 TEM images of the synthesized Si-C-Fe hybrid microspheres at low (a) and high (b) magnification; (c) is local magnification of (b).

Fig. 9 Nitrogen adsorption-desorption isotherms and the corresponding pore-size distributions for the synthesized Si-C-Fe hybrid microspheres.

Fig. 10 Plots of magnetization, M , versus external applied magnetic field, H , at 300 K, for the synthesized Si-C-Fe hybrid microspheres.

Fig. 11 (a) UV-vis absorption spectra during Si-C-Fe hybrid microspheres promoted reduction of 4-NP; (b) A_t/A_0 as a function of reaction time; (c) linear relationship of $\ln(A_t/A_0)$ as a function of time; and (d) the recyclability of the Si-C-Fe hybrid microspheres.

Fig. 12 The calculated structures of 4-NP, sp^2 carbon domain and their mixture using DFT.

Table 1 The binding energy (B.E.) of chemical bonds of ferrocene-modified PDVB microspheres.

Si 2p		C 1s				Fe 2p	
Bond	B.E. (eV)	Bond	B.E. (eV)	Bond	B.E. (eV)	Bond	B.E. (eV)
Si-C	100.3	C=C	284.5	C-OH	286.8	Fe 2p _{3/2}	708.0
C-Si-O	102.1	C-C	285.2	COO	289.1	Fe 2p _{1/2}	720.7
--	--	C*-C=O	286.1	π - π^*	290.8	--	--

Table 2 The binding energy (B.E.) of chemical bonds of the synthesized Si-C-Fe hybrid microspheres.

Si 2p		C 1s				Fe 2p _{3/2}	
Bond	B.E. (eV)	Bond	B.E. (eV)	Bond	B.E. (eV)	Bond	B.E. (eV)
Si-C	101.1	C-Si	283.1	C-O-Si	287.1	Fe ⁰	707.5
Si-O	102.7	C=C	284.1	C=O	288.3	Fe ²⁺	709.9
--	--	C-C	285.0	COOH	289.5	FeOOH	712.0
		C-OH	285.8				

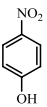
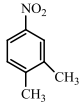
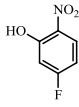
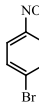
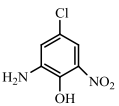
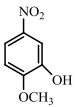
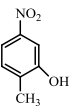
Table 3 Comparison of catalytic performance by various metal nanocatalysts for the reduction of 4-nitrophenol.

Catalyst	C_{NaBH_4}/C_{4-NP}	Temperature ^a (°C)	k_{nor} (s ⁻¹ mM ⁻¹)	TOF (s ⁻¹)	Reference
Si/C/Fe microspheres	100	RT	0.326	0.163	This work
Ag/Fe ₃ O ₄ @C	125	25	0.0030	--	38
Pd/C	240	RT	0.049	0.082	39
carbon nanofibers/Ag	42	25	0.0364	--	31
Pt-poly-emulsion monolith	11300	RT	0.0051	--	40
SiO ₂ @Au	117	RT	0.0388	0.049	41
Fe ₃ O ₄ @TiO ₂ /Au	83	25	1.656	0.121	42
CuMg ₂ Al/reduced graphene oxide	125	RT	1.838	0.136	69

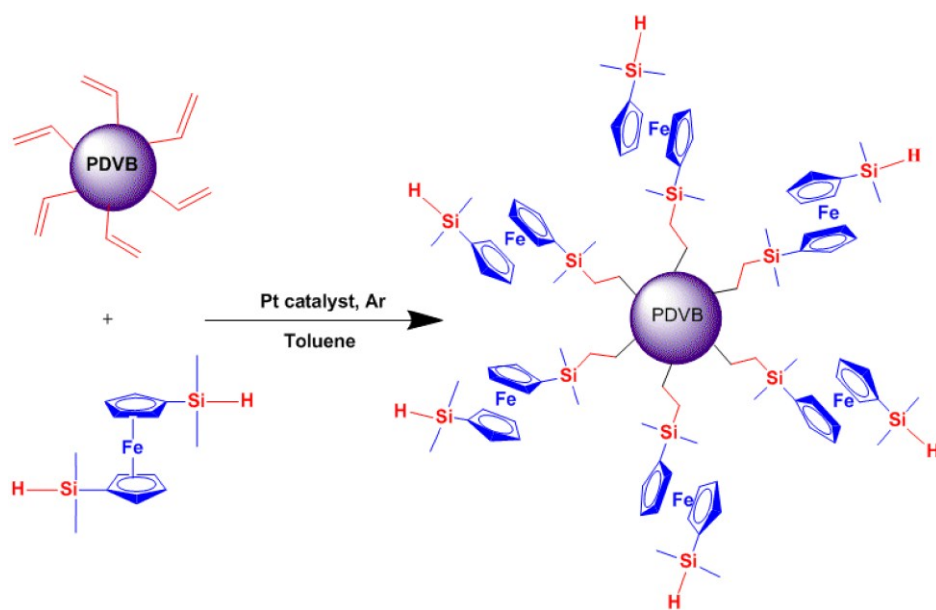
^a RT is at room temperature

Table 4 Catalytic performance of Si-C-Fe hybrid microspheres in the reduction of various nitroarenes (to the corresponding amines).^a

View Article Online
DOI: 10.1039/C7TA01156C

Entry	Substrate	Amount of Catalysts (mg)	$n_{\text{nitrobenzenes}}$ (mmol)	k_{nor} ($\text{s}^{-1} \text{mM}^{-1}$)	TOF (s^{-1})
1		4	6×10^{-3}	0.326	0.163
2		4	6×10^{-3}	0.044	0.013
3		2	5×10^{-3}	0.381	0.125
4		2	1×10^{-3}	0.510	0.025
5		4	3×10^{-3}	0.278	0.042
6		4	6×10^{-3}	0.075	0.038
7		4	6×10^{-3}	0.264	0.132

^a the amount of reactants in the entries 3-5 are limited by their solubilities.

**Scheme 1**

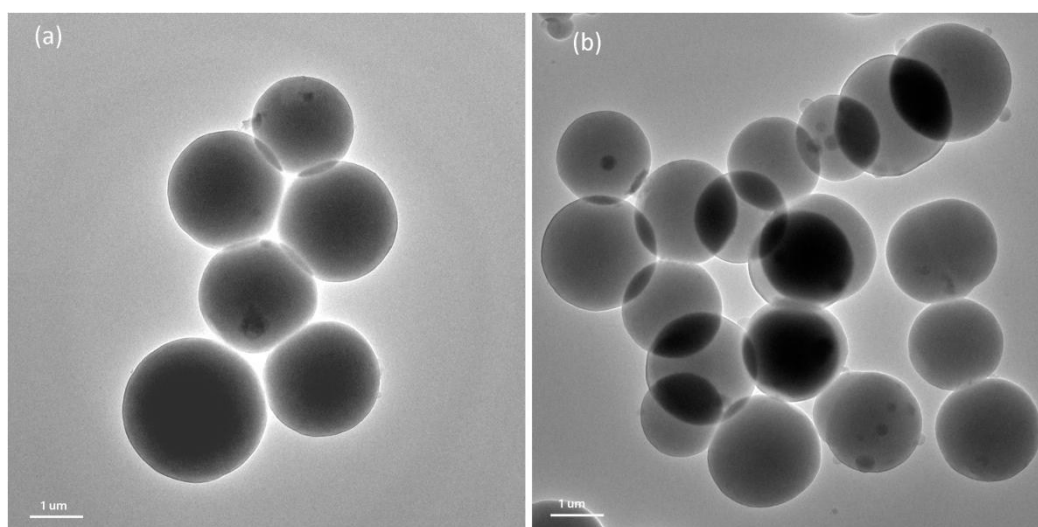


Fig. 1

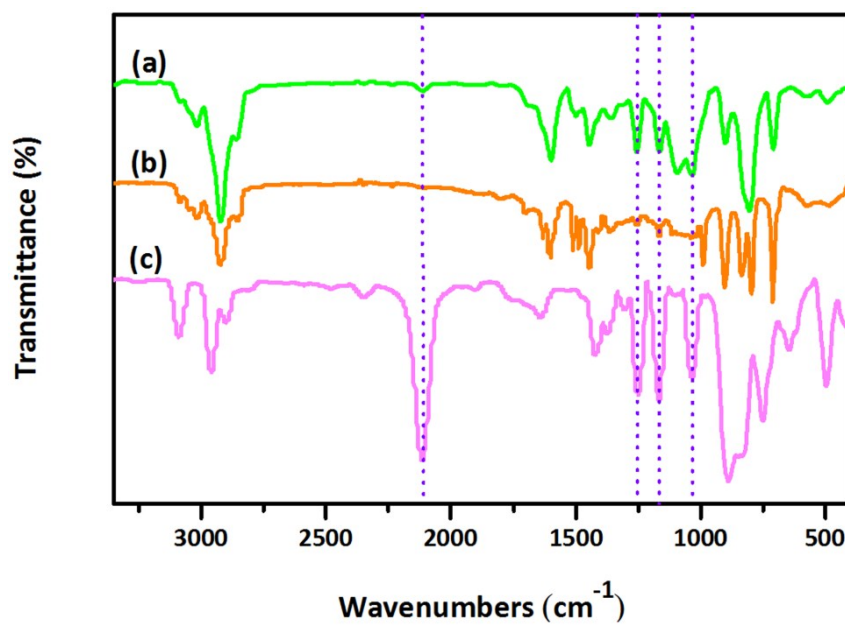


Fig. 2

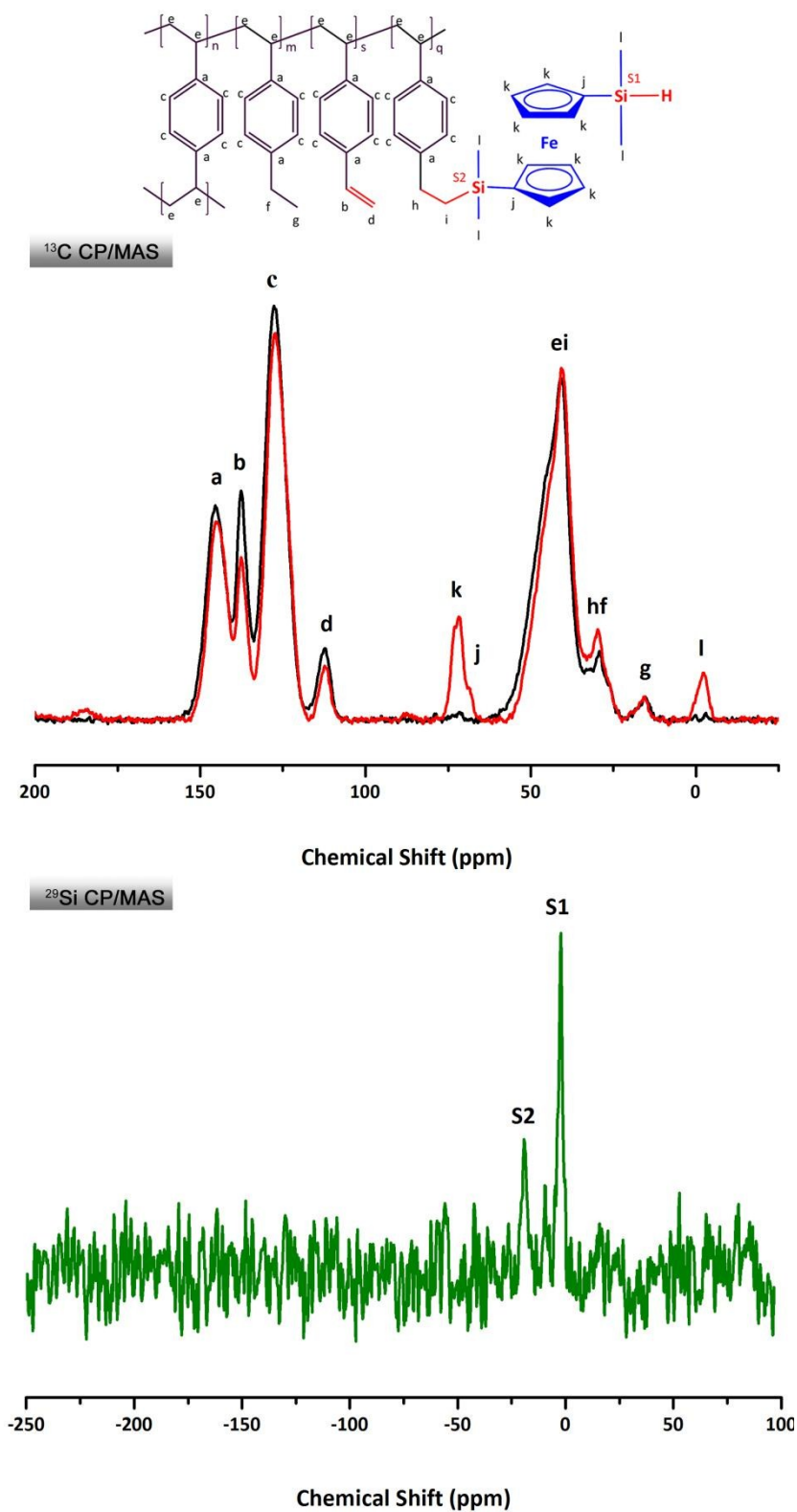


Fig. 3

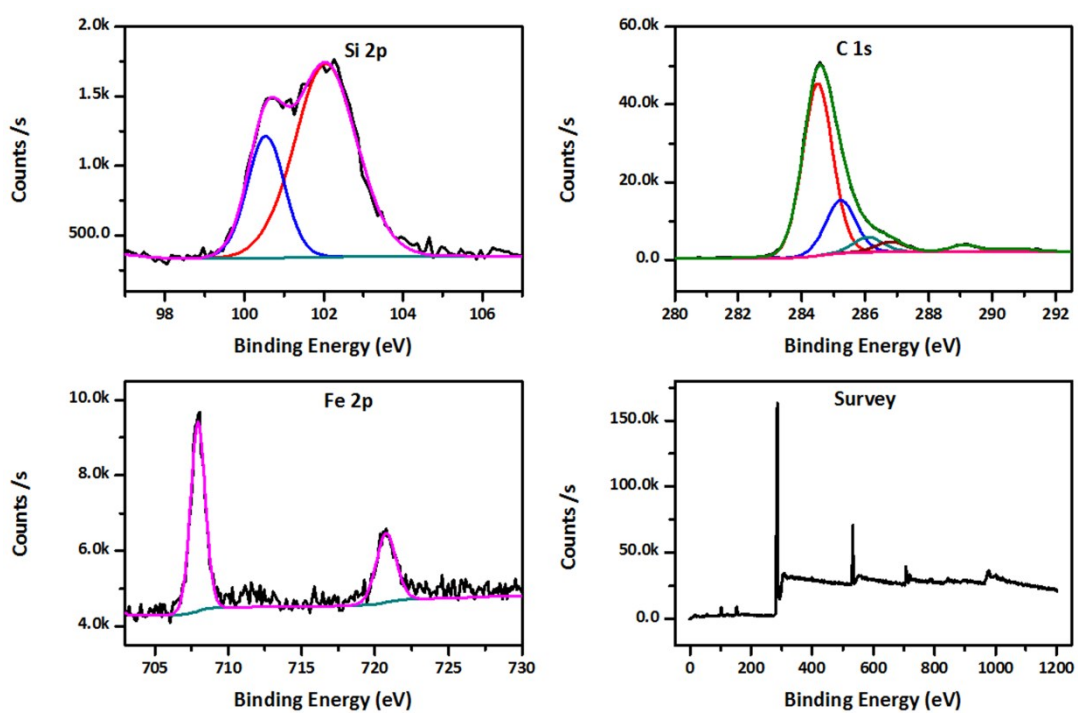
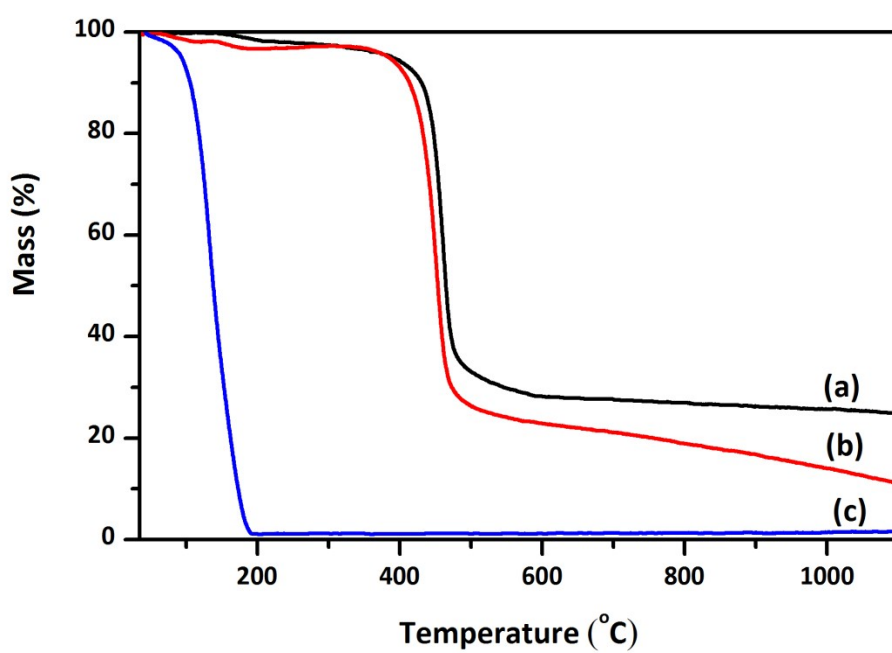


Fig. 4

**Fig. 5**

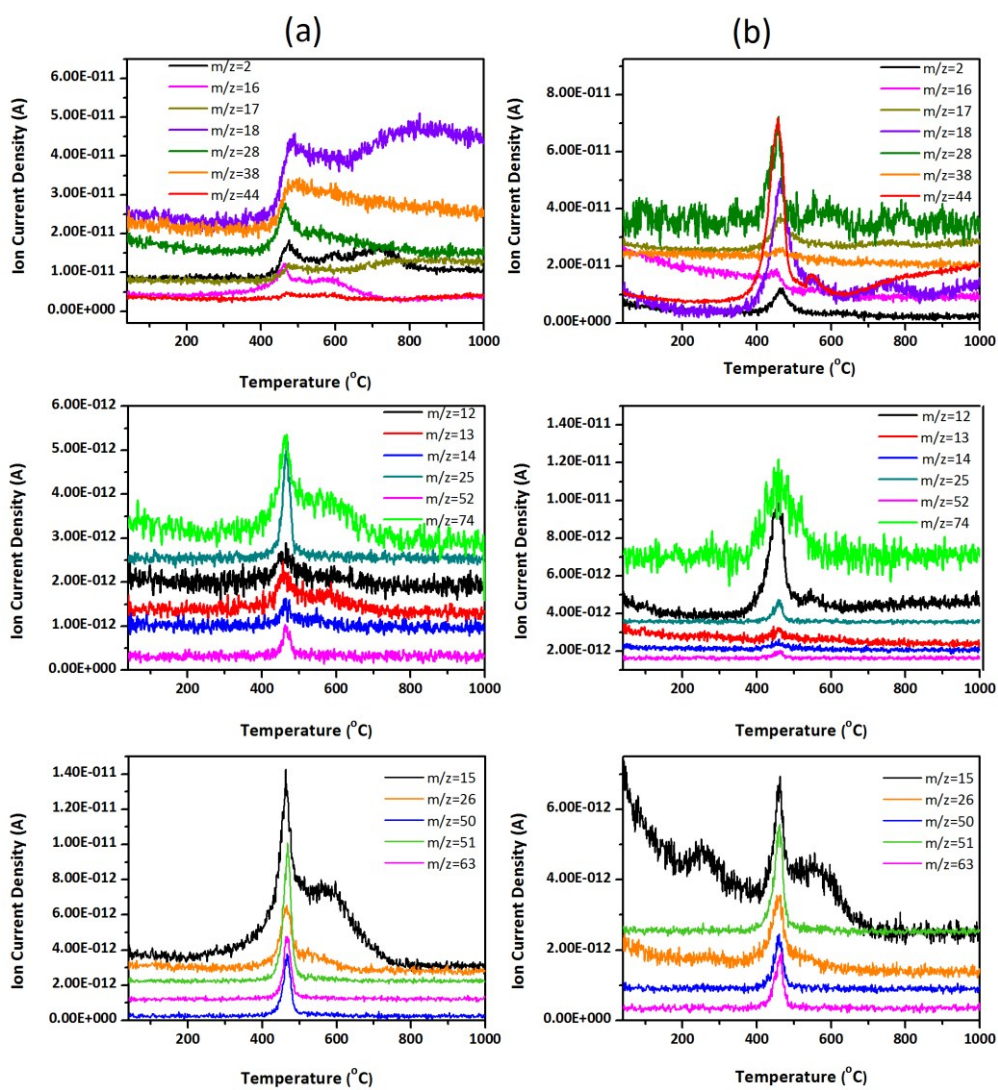


Fig. 6

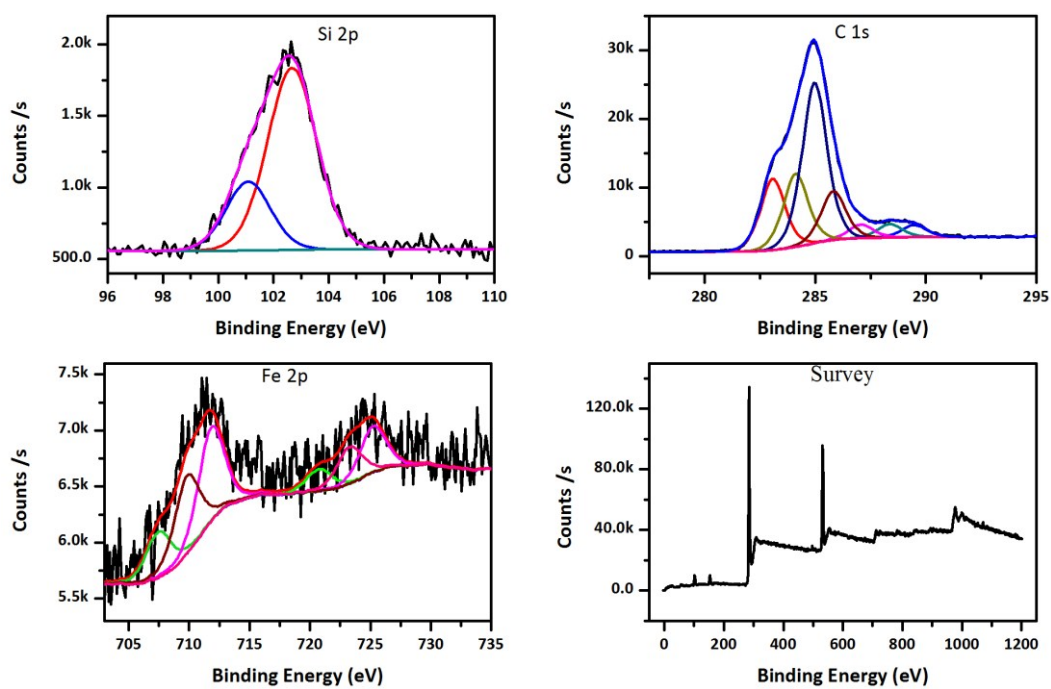
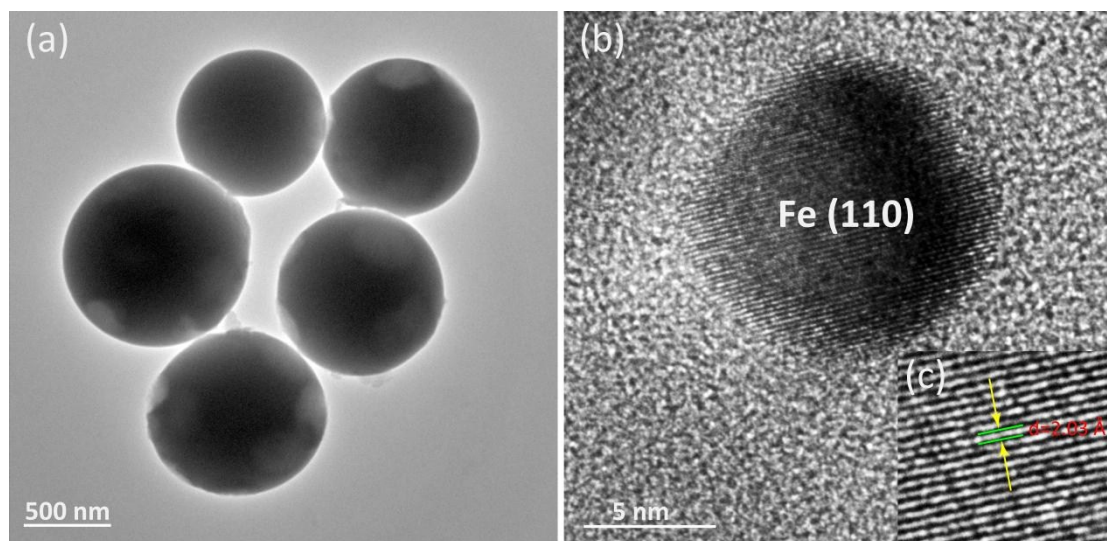


Fig. 7

**Fig. 8**

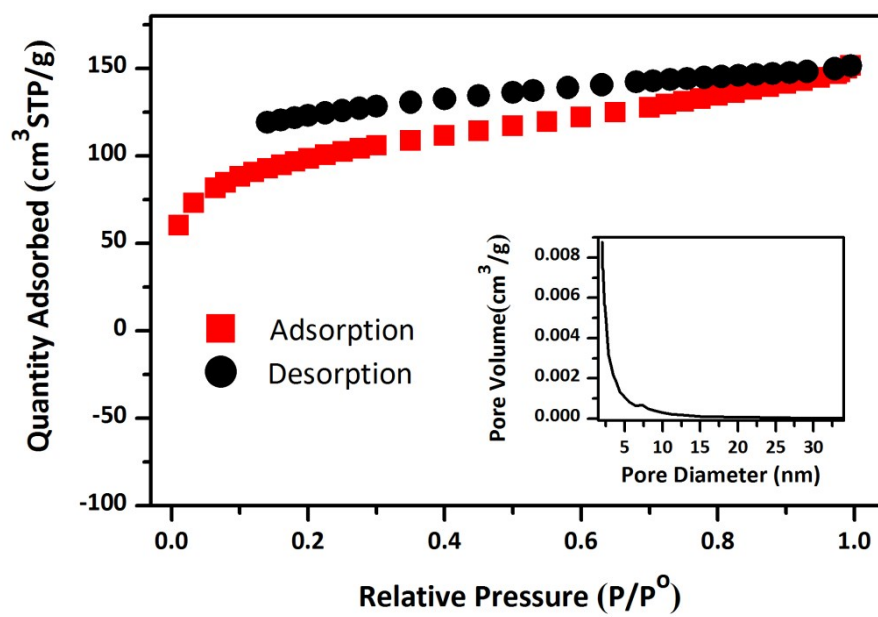
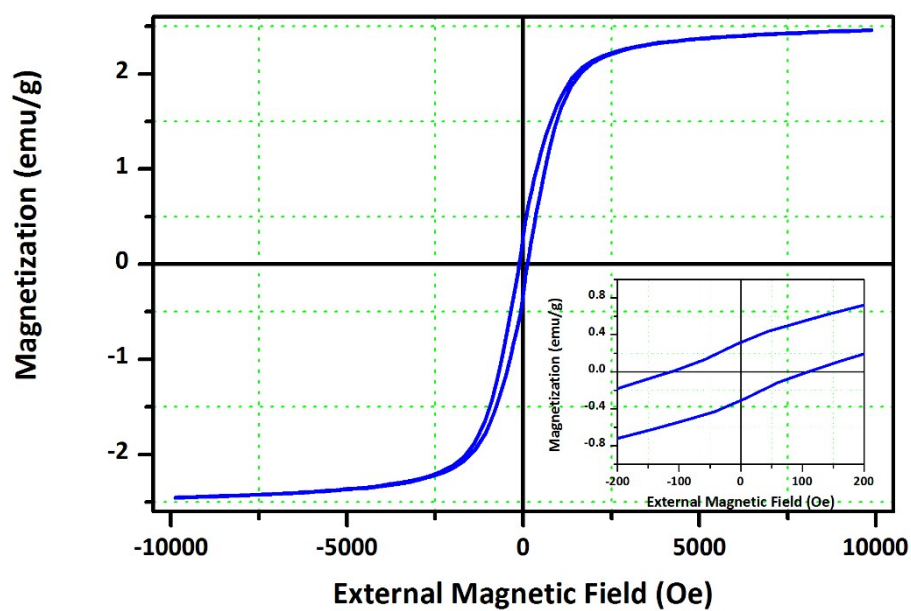


Fig. 9

**Fig. 10**

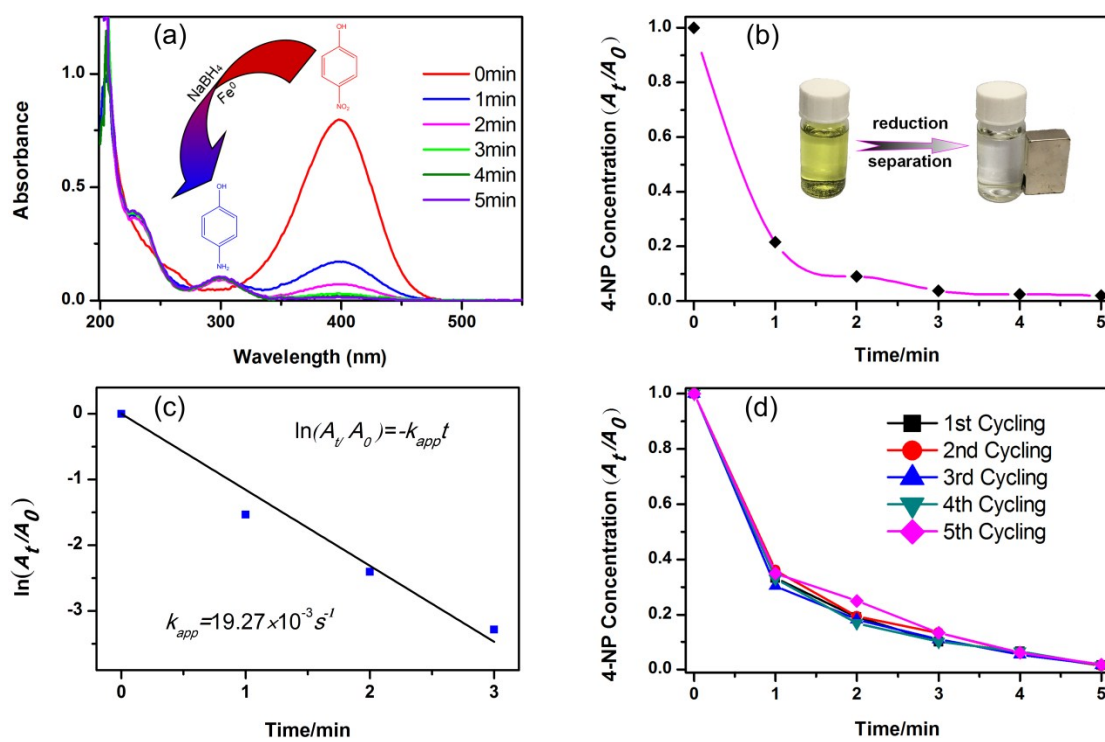
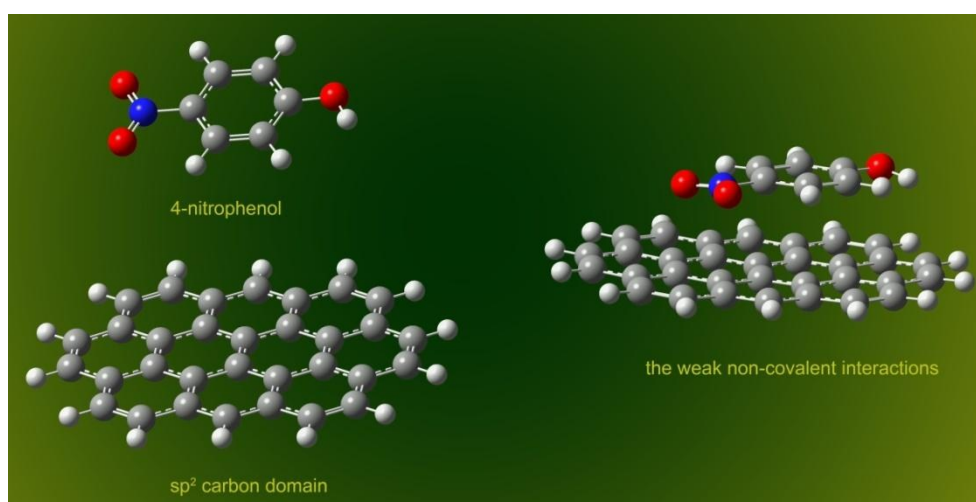


Fig. 11

**Fig. 12**